

Spinel-based ceramic membranes coupling solid sludge recycling with oily wastewater treatment

Chen, Mingliang; Zhu, Li; Chen, Jingwen; Yang, Fenglin; Tang, Chuyang Y.; Guiver, Michael D.; Dong, Yingchao

DOI

[10.1016/j.watres.2019.115180](https://doi.org/10.1016/j.watres.2019.115180)

Publication date

2020

Document Version

Accepted author manuscript

Published in

Water Research

Citation (APA)

Chen, M., Zhu, L., Chen, J., Yang, F., Tang, C. Y., Guiver, M. D., & Dong, Y. (2020). Spinel-based ceramic membranes coupling solid sludge recycling with oily wastewater treatment. *Water Research*, 169, Article 115180. <https://doi.org/10.1016/j.watres.2019.115180>

Important note

To cite this publication, please use the final published version (if applicable).
Please check the document version above.

Copyright

Other than for strictly personal use, it is not permitted to download, forward or distribute the text or part of it, without the consent of the author(s) and/or copyright holder(s), unless the work is under an open content license such as Creative Commons.

Takedown policy

Please contact us and provide details if you believe this document breaches copyrights.
We will remove access to the work immediately and investigate your claim.

Spinel-based Ceramic Membranes Coupling Solid Sludge Recycling with Oily Wastewater Treatment

Mingliang Chen^{a,b}, Li Zhu^c, Jingwen Chen^a, Fenglin Yang^a, Chuyang Y. Tang^d, Michael D. Guiver^e, Yingchao Dong^{a*}

^aKey Laboratory of Industrial Ecology and Environmental Engineering (Ministry of Education, MOE), School of Environmental Science and Technology, Dalian University of Technology, Dalian 116024, China

^bDepartment of Sanitary Engineering, Faculty of Civil Engineering and Geosciences, Delft University of Technology, P.O. Box 5048, 2600 GA Delft, The Netherlands

^cEngineering Research Center of Environmental Materials and Membrane Technology of Hubei province, School of Materials Science and Engineering, Wuhan Institute of Technology, Wuhan, P. R. China

^dDepartment of Civil Engineering, The University of Hong Kong, Pokfulam, Hong Kong S.A.R., China

^eState Key Laboratory of Engines, and Collaborative Innovation Center of Chemical Science and Engineering (Tianjin), Tianjin University, Tianjin 300072, P R China

Corresponding authors:

Dr. Yingchao Dong, Professor

Key Laboratory of Industrial Ecology and Environmental Engineering (Ministry of Education, MOE), School of Environmental Science and Technology, Dalian University of Technology, Dalian 116024, China

Tel: +86-411-84706328 E-mail: ycdong@dlut.edu.cn

© 2020 Manuscript version made available under CC-BY-NC-ND 4.0 license
<https://creativecommons.org/licenses/by-nc-nd/4.0/>

Abstract

Highly efficient and economic treatment of wastewater sludges and wastewaters in one way is a challenging issue in the water treatment field. Herein we present a waste-to-resource strategy for rational fabrication of low-cost ceramic membranes, which simultaneously addresses the treatment of heavy metal-laden sludges and the separation of oil-in-water (O/W) emulsions. A thermal conversion mechanism is proposed for complicated reactions between simulated nickel-laden wastewater sludge and bauxite mineral. In addition to full stabilization and recycling of heavy metal wastewater sludges, rational tailoring of ceramic membrane structures can also be realized to achieve high water flux, favorable mechanical and surface properties. With rational structure design, the tailored spinel-based ceramic membranes exhibited high rejection and high flux ($7473 \text{ LMH}\cdot\text{bar}^{-1}$) simultaneously for separation of oily wastewater, outperforming other reported state-of-the-art ceramic membranes. The membrane fouling mechanism revealed the dominance of cake layer formation at low cross flow velocities, while a combined model of cake layer formation and pore blocking dominated membrane fouling at high cross-flow velocities. The proposed strategy can be potentially extended toward design of functional ceramic membranes derived from other heavy metal wastewater sludges and for other water treatment applications.

Keywords: Wastewater sludge; Ceramic membrane; Oily wastewater; High flux; Membrane fouling.

1. Introduction

Sludges generated from industrial wastewater treatment often contain elevated concentrations of heavy metals such as copper, nickel, zinc, chromium and manganese, which are detrimental to the environment and human health (Duruibe et al., 2007). These hazardous heavy-metal containing sludges are often disposed of in controlled landfills by treating with cements (Song et al., 2013), a method which is generally considered unsustainable in the long run. Sorption and cementation, the dominate mechanisms for heavy metal stabilization in controlled landfills, are not sufficient in preventing their leaching in acidic environments (Christensen et al., 2001; Slack et al., 2005). Consequently, a more effective heavy metal stabilization strategy is highly needed.

Compared to landfill treatment, the thermal conversion method offers more reliable heavy metal stabilization combined with a significantly reduced risks of leaching. This method involves the formation of stable ceramic phases such as spinel, during which heavy metals are incorporated irreversibly into acid-stable crystalline phases (Shih et al., 2006b; Tang et al., 2011a; Tang et al., 2011b). For example, Shih et al. investigated the stabilization of nickel with γ -alumina, kaolinite and hematite. All the precursors showed high nickel incorporation efficiency when sintered at above 1250 °C (Shih et al., 2006a). The same group also studied the stabilization of copper and zinc in other work using the same method. It was found that these heavy metals can be efficiently stabilized in the spinel phases as well (Tang et al., 2011a). In addition, this method appeared to be feasible for real wastewater heavy metal-laden sludges (Tang et al., 2011b). Therefore, spinel-based heavy metal stabilization method can be potentially used to prepare a variety of ceramic products from metal-laden sludges.

In recent years, ceramic membranes have been increasingly employed for wastewater treatment because of their small footprint, no chemical pretreatment, low energy consumption and high removal efficiency (Dong et al., 2009; Hua et al., 2007; Lee and Kim, 2014; Salahi et

al., 2010). Due to their higher mechanical, chemical and thermal stability and anti-fouling property, ceramic membranes generally perform better than polymeric membranes, particularly for harsh applications such as the separation of oil/water (O/W) emulsions (Abadi et al., 2011; Dong et al., 2018; Zhu et al., 2016; Zhu et al., 2019). Inspired by the spinel-based stabilization method, a waste-to-resource strategy is proposed for the rational fabrication of low-cost ceramic membranes which simultaneously addresses the treatment of heavy metal laden sludges and the separation of O/W emulsions.

In the current study, we systematically elucidate the formation mechanism of acid-stable NiAl_2O_4 spinel during the preparation of hollow fiber ceramic membrane (HFCM) using a mixture of synthetic nickel-laden wastewater sludge (NiO) and naturally abundant bauxite mineral. Two different membrane structures (sandwich-structured HFCM (SS-HFCM) vs. long finger-like pore structured HFCM (LFS-HFCM)) were studied for O/W emulsion separation under various operating conditions. We show that the excellent surface hydrophilicity induced by the abundant metal hydroxyl groups combined with the special structural features of the LFS-HFCM led to high membrane permeate flux, outperforming other existing ceramic membranes. The current study provides a rational and cost-effective approach for the design and fabrication of high-performance ceramic membranes.

2. Experimental section

2.1. Materials and chemicals

Abundantly available bauxite (after 1600 °C calcination, Yangquan, Shanxi Province, China) and NiO (99%, analytical reagent, Sinopharm Chemical Reagent Co., Ltd., China) were used as the raw materials for the preparation of low-cost spinel-based hollow fiber ceramic membranes. The chemical composition of bauxite is shown in [Table S1 \(Supporting Information \(SI\)\)](#), determined by semi-quantitative X-ray fluorescence spectroscopy (XRF, Axios-Advanced, PAN3 analytical, The Netherlands). Other characterization results of bauxite such as phase composition and particle size distribution can be found in our recent publication (Dong et al., 2018). Polyethersulfone (PES, E2010, BASF Chemical Company, Germany) and N-methyl-2-pyrrolidinone (NMP, CP Grade, Sinopharm Chemical Reagent Co. Ltd., China) were used as the polymer binder and the solvent respectively, to prepare the mixed polymeric solutions. Polyvinylpyrrolidone (PVP K-30, 45000Da, Sinopharm Chemical Reagent Co. Ltd., China) was used as the additive. Deionized (DI) water was used as the internal coagulant while the mixtures of tap-water/ethanol with different ethanol volumes (0%, 30%, 60% and 90%) were used as the external coagulants, to accomplish the gelation and phase conversion processes of spun hollow fiber precursors.

2.2. Membrane fabrication

The spinel-based HFCMs were prepared by a dry-wet spinning technique ([Fig. S1](#)), involving immersion-induced phase inversion and drying-sintering processes. Systematic optimization of various suspension compositions and spinning parameters were conducted ([Table S2](#)). The details of the preparation are described in [SI](#) and other literature (Dong et al., 2018).

2.3. Membrane characterization

The crystalline phases of calcined bauxite and sintered HFCMs (1000-1300 °C) were characterized by X-ray diffraction (XRD, DX-2700, Dandong Haoyuan Instrument Co., Ltd.,

China, Cu K α radiation, working voltage 40 kV, working current 30 mA, scanning speed of 5.0° (2 θ) · min⁻¹). Here, each phase present in the XRD patterns were semi-quantitatively analyzed based on the normalized reference intensity ratio (RIR) method (Chung, 1974). The details of this method can be found in our previous work (Chen et al., 2016). Microstructures of green and sintered HFCMs were visually observed using a scanning electron microscope (SEM, S-4800, Hitachi Ltd., Japan). Surface porosity of hollow fiber membranes was quantified by ImageJ software (Vasanth et al., 2011), where SEM images were processed into black and red regions, which present ceramic particles and membrane pores, respectively. Other characterizations such as mechanical strength, pore size distribution, fourier-transform infrared spectroscopy (FTIR), X-ray photoelectron spectroscopy (XPS), transmission electron microscopy (TEM), selected area electron diffraction (SAED) and pure water flux were described in SI.

2.4. O/W emulsion separation by HFCMs

Membrane separation experiments of synthetic O/W emulsion wastewaters (S1.3, SI) were carried out in a laboratory-made crossflow filtration apparatus (Fig. S3). The O/W emulsion with a concentration of 500 mg·L⁻¹ was prepared by suspending a certain amount of oil into deionized water, then ultrasonicated for about 12 h in a sonicator tank at a temperature of 25 °C. To stabilize the emulsion systems, a surfactant (sodium dodecyl sulfonate) with a concentration of 0.1g·L⁻¹ was added into the mixture. Afterwards, the mixtures were vigorously magnetically stirred for 48 h until they appeared turbid and milky white, indicating good stability and homogeneity. The size distributions of oil emulsion droplets were measured by a Malvern Mastersizer analyzer (Mastersizer 2000, Malvern Instruments Ltd., UK) and the stability of the emulsion could be maintained for several days (Fig. S2). The filtration was conducted under a constant trans-membrane pressure of 0.1 bar at three cross-flow velocities of 0.56 m·s⁻¹, 1.12 m·s⁻¹ and 1.67 m·s⁻¹, respectively. All the experiments were conducted at room temperature

(25 °C). Oil concentrations in the permeate samples varied with time were obtained by measuring the absorbance with 10 min interval. The permeate flux (J , $L \cdot m^{-2} \cdot h^{-1}$) and oil rejection (R) were calculated according to the following equations by weighing permeate every 10 min in a digital balance and by measuring absorbance in a UV-visible spectrophotometer (SPECORD250 PLUS, Analytik Jena, Germany), respectively.

$$J = \frac{V}{A \cdot \Delta t} \quad (1)$$

$$R = \frac{C_f - C_p}{C_f} \quad (2)$$

Where, A (m^2) is the effective membrane area, V (m^3) is the volume of permeate, Δt (s) is the sampling time, C_f ($mg \cdot L^{-1}$) and C_p ($mg \cdot L^{-1}$) are the concentrations of oil in feed and permeate, respectively.

After each separation run, the membranes were cleaned using the following protocol. The membranes were first washed with de-ionized water for 5 min, then with 1 wt. % NaOH solution for 30 min to remove the oil droplets adhered on the surface and in the porous structure. Subsequently, the membranes were washed with 1 wt. % HCl solution for 30 min and finally rinsed with de-ionized water for 5min.

3. Results and discussion

3.1. Recycling of wastewater sludge for spinel formation

In order to recycle heavy metals in wastewater sludge in an efficient and safe way, in this work, nickel oxide (simulated nickel-laden wastewater sludge) and bauxite are considered and sintered at high temperatures to produce ceramic membrane via the formation of a more stable spinel phase in ceramic matrix.

Formation evolution of the spinel phase is first confirmed by XRD analysis. [Figs. S4a](#) and [S4b](#) illustrate the XRD patterns and quantification of various phase contents of the spinel-based HFCMs sintered from 900 to 1300 °C for 2 h. There is no nickel aluminate spinel phase formed

in the samples sintered at temperatures below 1000 °C. After sintering at 1050 °C, NiAl₂O₄ spinel phase can be readily identified in the samples with a content of ~31 wt. % due to the solid-state reaction between nickel oxide and mullite or corundum. When further increasing the temperature up to 1100 °C, spinel becomes the dominant phase with a content as high as 88.4 wt. %, which is also indicated by the significantly increased reflection intensity of the spinel phase from 1050 to 1100 °C (Fig. S4a). Above 1150 °C, only NiAl₂O₄ spinel phase can be detected at ~100 wt.% content, meaning that nickel oxide fully reacted with corundum and mullite to effectively and completely realize its thermal conversion and stabilization above this temperature.

Morphology and structure of the individual spinel phase are also readily observed by electron microscopy characterization, including SEM, EDS, TEM. After 15 wt. % HF solution etching, both residual rod-like mullite and the formed octahedral NiAl₂O₄ spinel crystals can be visually observed by SEM (Fig. S4(c)), where the local chemical compositions were further determined by SEM-EDS analysis (Fig. S4(d)). The molar ratios of Al/Ni and Al/Si in the detected spinel and mullite crystals are 2.3 and 3.9, which are slightly higher than the theoretical values of 2 (NiAl₂O₄) and 3 (3Al₂O₃·2SiO₂) (Table S3), due to the influence of surrounding substances such as α -Al₂O₃ around the EDS-analyzed micro regions. The formation of NiAl₂O₄ spinel structure was further confirmed by TEM analysis (Fig. S4e), which also shows an octahedral morphology, as clearly observed in the SEM image (Fig. S4c). An individual grain was once again identified by the corresponding SAED patterns (Fig. S4f), which can be exclusively attributed to the NiAl₂O₄ phase, without any indications of residual NiO, which is in good agreement with the XRD results (Fig. S4a).

In acidic aqueous environment, after stabilization with bauxite, the leaching stability of NiAl₄ and NiAl₂ membranes is much better than that of NiO (Fig. S5). Compared with the other Ni-based spinel products stabilized using γ -Al₂O₃ and kaolinite, the as-formed nickel

aluminate spinel using bauxite as precursor in this study has excellent acidic stability (a low leaching level of 26 mg/L), which is much better (than γ - Al_2O_3) or at least comparable (with kaolinite) (Fig. S6a). More especially, using bauxite, lower stabilization cost can be realized (78% of γ - Al_2O_3 and 76% of kaolinite) due to lower stabilization temperature (1150 °C) and cheaper material cost (Table S4, Fig. S6b). All these characteristics fully indicate that bauxite mineral is a promising but cost-effective candidate for nickel thermal conversion.

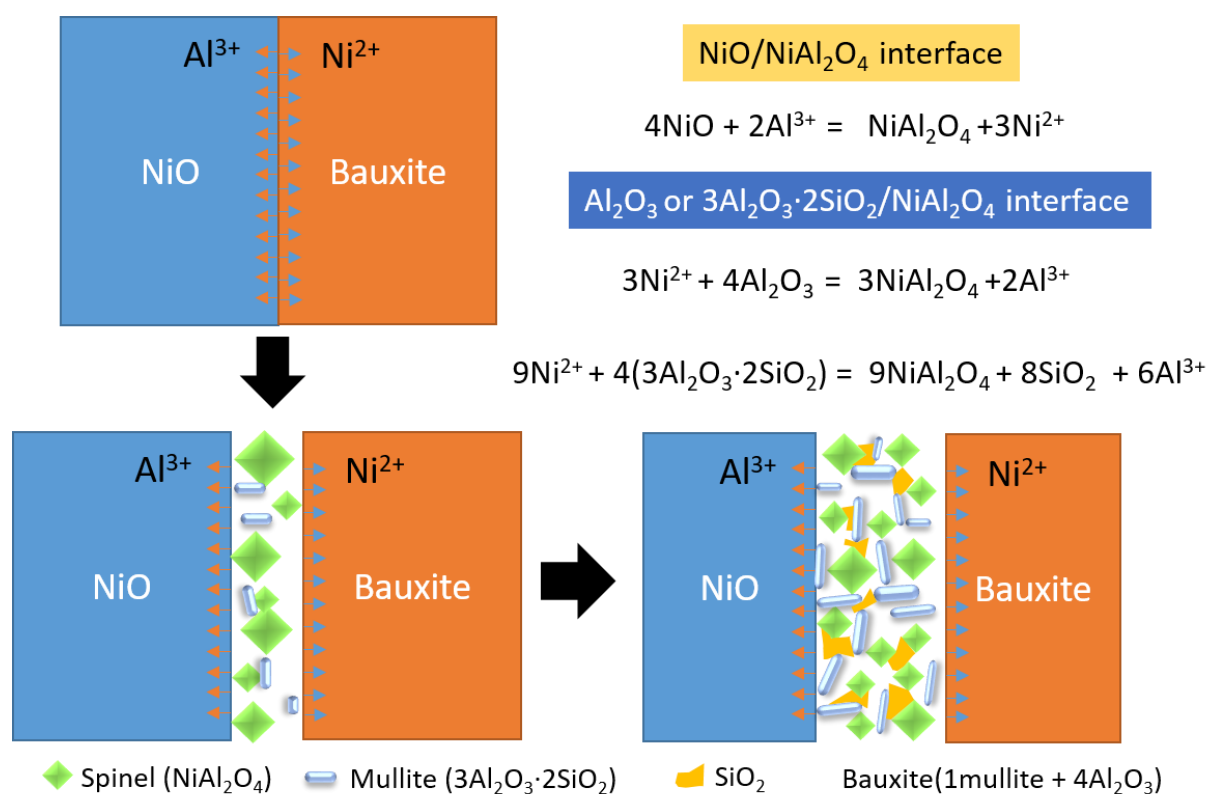


Fig. 1. Schematic diagram of thermal conversion reaction mechanism for spinel NiAl_2O_4 formation via high temperature reaction between NiO and bauxite mineral.

Revealing reaction paths of various phases is important to gain a deeper understanding of the thermal conversion mechanism, since minerals and wastes generally have complicated phase and chemical compositions. Based on the comprehensive detailed analysis of XRD and microscopy characterization (SEM, TEM and EDS), the thermal conversion mechanism of spinel NiAl_2O_4 is more clearly understood, as depicted in Fig. 1. The nucleation and subsequent growth of NiAl_2O_4 crystals begin from the solid interface between nickel oxide and bauxite

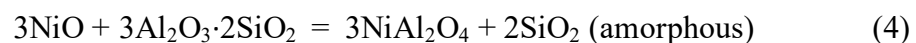
(both mullite and alumina) as two parent phases, where Ni and Al ions counter-diffused through spinel lattice to maintain continuous crystal growth. Three distinct stages can be identified for spinel NiAl_2O_4 formation from NiO and calcined bauxite (with mullite and corundum as crystalline phases) (Leblud et al., 1981). The first stage occurred between 1000 °C and 1050 °C, the reaction between NiO and $\alpha\text{-Al}_2\text{O}_3$ (eq 3) was much more favored as compared to that between NiO and thermally more stable mullite (eq 4), which is further fully evidenced by the unchanged phase content of mullite with increasing temperature (Fig. S4b).

1000-1050 °C



The second stage occurred at the temperature window of 1050-1150 °C. As the calcination temperature was increased to 1050 °C, the solid state reaction between mullite and NiO was initialized and then the growth rate of spinel increased more rapidly at this stage. Furthermore, the consumption of NiO for spinel formation sintered at 1050-1150 °C was more significant than that in the first stage (< 1050°C). This can be attributed to the acceleration of reaction rate of the two phases at higher temperatures. Also, amorphous silica produced by the reaction of mullite and NiO became liquid phase at this temperature and thus acted as a flux agent, thereby significantly facilitating mass transfer and phase reaction (Shih et al., 2006a). Therefore, a higher reaction rate occurred for corundum and nickel oxide.

1050-1150 °C



Above 1150 °C (the third stage), a complete transformation of nickel oxide into pure NiAl_2O_4 structure was accomplished while no residual corundum and mullite phases were found.

Chemical compositions of the precursors played an important role on morphology and size of the produced spinel. Mullite precursor facilitated greater mass transfer rates at high temperatures, thus resulting in more significant surface diffusion rate and faster reaction rate,

but smaller grain sizes (Fig. S4c). Compared with our previous studies about copper (Li et al., 2015a) and zinc (Li et al., 2015b), heavy metal stabilization with bauxite, the spinel phase formed in the NiO-bauxite system is more stable and proceeds without the generation or decomposition of intermediate phases in the reaction process (Table S5). Further discussion of our results and those with only γ -Al₂O₃ and kaolinite for stabilization of nickel-laden solid state wastes (Shih et al., 2006a; Shih et al., 2006b) was given in the Table S5, SI.

These above-mentioned results indicate that the method presented in this work appears to be feasible and promising not only for the highly efficient stabilization of nickel-laden wastewater sludge into spinel-based ceramic membranes at lower costs, but also disclosing a possible way to rationally design and prepare low-cost functional ceramic membranes via a waste-to-resource strategy, the latter will be further discussed in the following sections and SI.

3.2. Rational design of spinel-based ceramic membranes

The HFCMs with highly controllable structure morphology consisting of an adjustable sponge-like region and finger-like macro-voids could be precisely designed and prepared by the dry-wet spinning technique, which is an efficient way to prepare a highly asymmetric membrane in one step (Fig. 2) (Wei et al., 2008). To obtain high performance robust ceramic membranes with ideal structures featuring suitable pore size, high permeability and acceptable mechanical properties, dry-wet spinning parameters (such as solid state loading, air gap and external coagulant components) and sintering temperature were comprehensively studied and discussed in detail (section S3, SI) to obtain optimized structural morphology and properties for subsequent highly efficient O/W emulsion separation. A higher solid-state loading promoted the formation of more regular lumen structures in the fibers (Fig. S7). A longer air-gap distance increased the amount of long inner finger-like macro-voids (Fig. S8). Increasing the content of ethanol in the external coagulant further significantly promoted the formation of morphology with longer and larger inner finger-like macro-voids (Fig. S9). Membrane structures featuring

long and large-sized finger-like macro-voids endow high flux with low permeation resistance. Two representative membranes: SS-HFCM (fiber 3) and LFS-HFCM (fiber 7) with typically different cross-sectional structures are presented for further study.

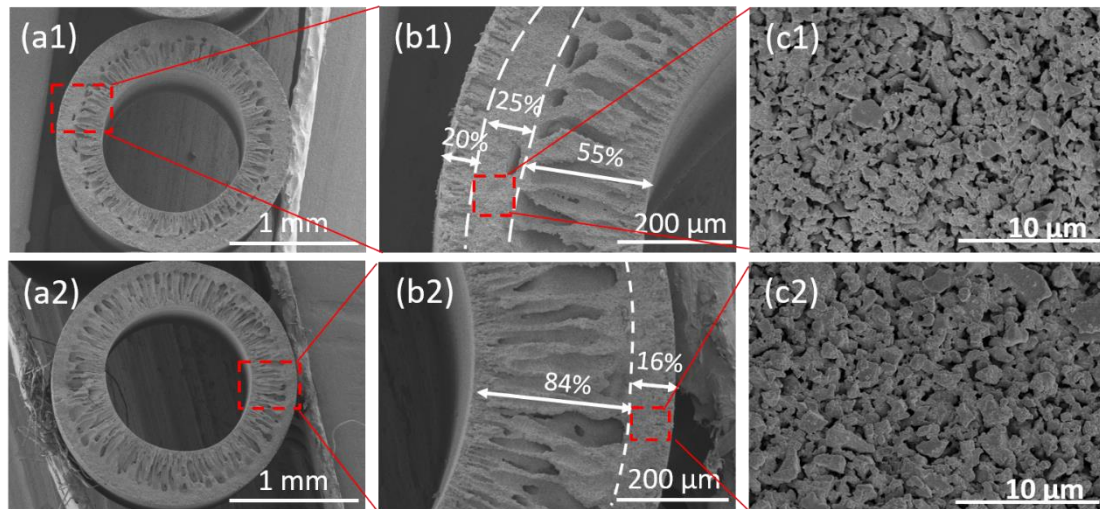


Fig. 2. Cross sectional SEM images of HFCMs with different magnifications, sintered at 1250 °C for 2 h: SS-HFCM (a1-c1) and LFS-HFCM (a2-c2). SS-HFCM and LFS-HFCM were prepared with pure water and 60 vol. % ethanol and 40 vol. % water mixture as external coagulant at a fixed air-gap distance of 15 cm, bore fluid flow rate of 20 mL·min⁻¹ and solid state loading of 60 wt. %, respectively.

The finger-like macro-voids originate from the inner, or outer or both inner/outer surfaces while the sponge-like area is formed in the intermediate area or on one side, which provides the majority of mechanical strength and separation function. By comparing SS-HFCM with LFS-HFCM, it can be concluded that the composition of external coagulant has a great effect on the distribution and ratio of sponge-like area and finger-like macro-voids in the cross section of hollow fiber membrane (Kingsbury and Li, 2009). LFS-HFCM with 60 vol. % ethanol in the external coagulant has much longer and larger-sized inner finger-like macro-voids (84%) than SS-HFCM (55%), obtained by using pure water as external coagulant. The sponge-like area of LFS-HFCM (16%) is thinner than that of SS-HFCM (25%), which significantly reduced the permeation resistance with the shorter transport path, showing comparable pore size but higher water flux (Figs. 3a and 3b). The average pore size of LFS-HFCM (0.35 μm) is very slightly

smaller than or comparable with that of SS-HFCM (0.36 μm) (Fig. 3a), which are in the microfiltration category. However, the pure water flux (Fig. 3b) of LFS-HFCM is almost two times higher than that of SS-HFCM at all cross-flow velocities. This can be attributed to the highly asymmetric structure of LFS-HFCM membrane with a very high finger-like/sponge-like ratio of ~ 5.25 (~ 3 for SS-HFCM), which significantly reduced the water permeation path with lower mass transport resistance. Similar results were reported by Zhang (Zhang et al., 2010) where YSZ (yttria-stabilized zirconia) hollow fiber membranes with long finger-like macrovoids were fabricated by the dry-wet spinning method using ethanol as an external coagulant. The surface porosities of LFS-HFCM are always higher than those of SS-HFCM at all sintering temperatures, whereas lower but acceptable bending strengths of LFS-HFCM are observed than those of SS-HFCM except for 1300 $^{\circ}\text{C}$. After sintering at 1250 $^{\circ}\text{C}$, besides high water flux, LFS-HFCM has a high surface porosity of $50.92 \pm 3.2\%$, and sufficient mechanical strength (35.64 ± 6.31 MPa) for separation applications (Fig. S11).

Understanding the surface property of ceramic membranes is important for O/W emulsion separations. Metal oxides with abundant MeO-H (Me=Ni, Al, Si, Ti etc.) groups are considered to be all hydrophilic due to chemisorption or hydrogen-bond interactions between MeO-H group and water molecules (Lu et al., 2016). The water contact angle of LFS-HFCM is 46° , which indicates that the spinel-based HFCMs are very hydrophilic due to the inherent surface Ni-OH and Al-OH groups (Fig. 3d). The surface metal-hydroxyl groups are further confirmed by FT-IR with a characteristic IR stretching vibration at 2410 cm^{-1} (Fig. 3c). Thus, during water treatment, metal hydroxyl groups on the membrane surface readily bond with a monolayer of water molecules. This hydrophilic (oleophobic) membrane surface characteristic is very beneficial for the treatment of O/W emulsions due to the low membrane fouling propensity of oil droplets (Obaid et al., 2017).

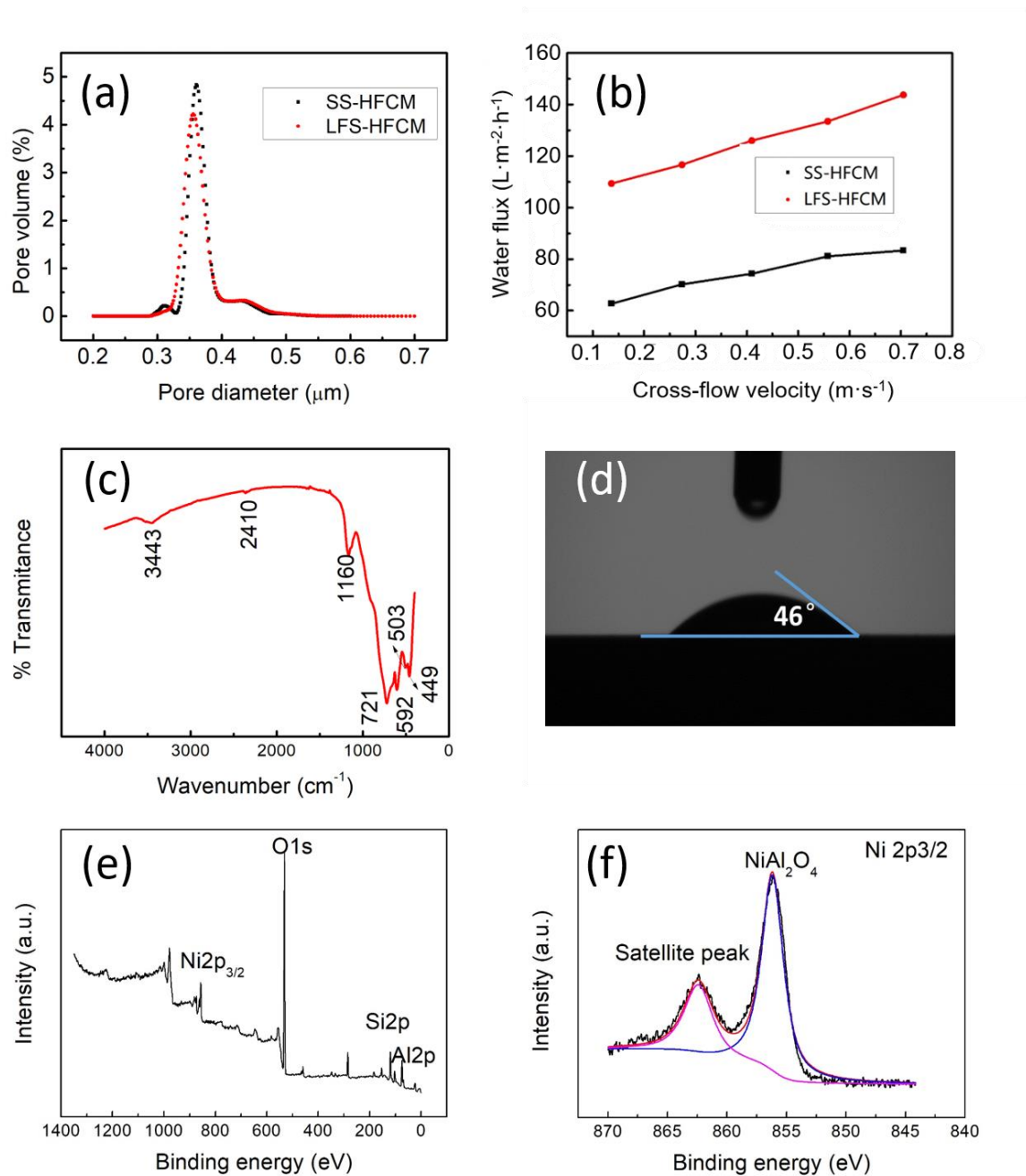


Fig. 3. Pore size distribution (a) and pure water flux (b) of SS-HFCM and LFS-HFCM sintered at 1250 °C for 2 h, (c) FT-IR spectra, (d) water contact angle, (e) XPS survey Al K α photoelectron spectrum and (f) XPS Ni $_{2p_{3/2}}$ spectrum of LFS-HFCM sintered at 1250 °C for 2 h.

Figs. 3e and **3f** give the XPS survey spectra of LFS-HFCM and the corresponding binding energies (BEs) of the Ni 2p $_{3/2}$ level. The Ni 2p $_{3/2}$ primary peak is positioned within a BE range of 856.0–856.5 eV and a satellite peak at 862.4–862.8 eV (Zhang et al., 2017). It is noted that the BE of Ni 2p $_{3/2}$ in pure NiO is \sim 854.5 eV (Guo et al., 2004), while for NiAl $_2$ O $_4$ spinel the

BE of Ni 2p_{3/2} appears at ~856.1 eV. Again, this illustrates that Ni²⁺ ions were completely chemically incorporated into the spinel lattice to achieve heavy metal stabilization during the high temperature sintering of ceramic membranes, as proven in the XRD patterns of Fig. S4a. The other XPS spectra such as O 1s, Al 2p and Si 2p are shown in Fig. S12. The O1s spectrum shows the presence of four different oxygen species. In addition to bulk oxygen in crystal structures of ceramic membranes (spinel and mullite), the surface of LFS-HFCM contains hydroxyl groups (9.93%) with an O1s binding energy of 532.1 eV, which is consistent with FT-IR results, further confirming the inherent hydrophilic characteristic of the prepared ceramic membranes.

3.3. Separation performance and membrane fouling mechanism

3.3.1. Effect of cross-flow velocity on permeate flux and oil rejection

In general, the attachment strength between hydrophobic organic compounds (such as oil droplets) and membrane surface is determined largely by their surface structure characteristic (Prince et al., 2016). Because of the hydrophilicity (WCA = 46°) of the spinel-based ceramic membrane surface, water molecules transit through the membrane surface and then enter into the pores more readily than hydrophobic oil droplets (Li and Elimelech, 2004). O/W emulsion separation experiments with a feed containing 500 mg·L⁻¹ machine oil, using SS-HFCM and LFS-HFCM, demonstrated different flux and oil rejection behavior (Fig. 4). Both fiber membranes experience a rapid permeate flux decline during the first 10 min, which could be attributed to the initial formation of a fouling layer at the membrane surface (Ahmad et al., 2005; Chen et al., 2016). Then, the permeate flux declines more gradually before reaching a steady value after about 100 min, indicating a stable dynamic oil layer was formed. Flux declines are the result of increasing fouling resistance, caused by the formation of a dynamic oil layer and concentration polarization on the membrane surface, and pore blocking within the porous ceramic structure (Vasanth et al., 2013). After a certain filtration time, the thickness of oil layer

did not increase further due to the hydrodynamic action of cross-flow and consequently the flux was stable thereafter. An increase in cross-flow velocity enhances permeate flux dramatically during the separation process (Fig. 4a), while a lower oil rejection is observed during the first 50 min (Fig. 4b). The initial permeate flux for LFS-HFCM increases from 316 to 747 LMH with an increase in cross-flow velocity from 0.56 to 1.67 m·s⁻¹. Higher cross-flow velocities increase turbulence and mass transfer coefficient inside the membrane tube, consequently mitigating concentration polarization on the ceramic membrane surface. Moreover, increasing cross-flow velocity contributes to an increase in the shear force of the feed fluid, thus significantly inhibiting the accumulation of oil droplets on the membrane surface and further diminishing the thickness of the oil fouling layer, which acts as an additional barrier to reject oil droplets (Kumar et al., 2015). In the whole separation run, the flux of LFS-HFCM is always higher than that of SS-HFCM (Fig. 4a), due to its more permeable structure consisting of a thinner sponge-like region and longer finger-like macro-voids, which reduce permeation resistance significantly (as clearly observed in Fig. 2b2) (Zhang et al., 2010). LFS-HFCM maintains a slightly decreased, but still high stable oil rejection of ~99.51% after 50 min when a stable oil cake layer is steadily formed (Fig. 4c). The higher rejection of SS-HFCM is ascribed to its thicker sponge-like separation layer, resulting in a longer permeation path and a higher adsorption of oil droplets inside the membrane pores at the beginning of the filtration process. Thus, LFS-HFCM shows better O/W separation performance than SS-HFCM in terms of permeate flux owing to its superior microstructure morphology. After filtration by LFS-HFCM at a cross-flow velocity of 1.67 m·s⁻¹, the permeate becomes visually cleaner with very low turbidity (like pure water), as compared to the feed (Fig. 4c). In order to mitigate membrane fouling for flux recovery, unlike polymeric membranes, a simple chemical cleaning method (1 wt. % NaOH and 1 wt. % HCl) was applied on the more robust ceramic membrane for flux regeneration. After cleaning, the flux at different cross-flow velocities were recovered

efficiently. The recovery rate of flux for LFS-HFCM at a cross-flow velocity of $1.67 \text{ m}\cdot\text{s}^{-1}$ was as high as $\sim 90\%$ of original flux.

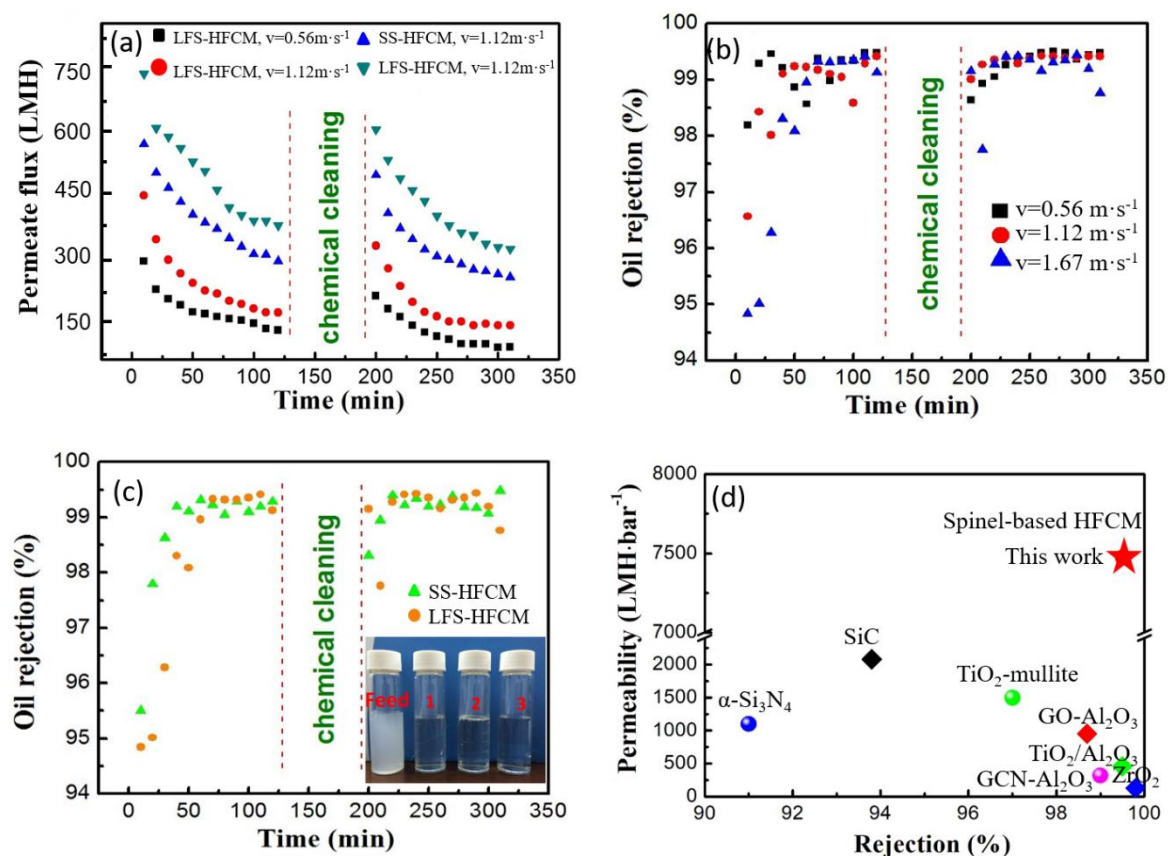


Fig. 4. Spinel-based HFCMs for O/W emulsion separation, (a) Time-dependent permeate fluxes before and after chemical cleaning for SS-HFCM and LFS-HFCM sintered at $1250 \text{ }^\circ\text{C}$ at different cross-flow velocities ranging from 0.56 to $1.67 \text{ m}\cdot\text{s}^{-1}$, (b) variation of oil rejection for LFS-HFCM at different cross-flow velocities ranging from 0.56 to $1.67 \text{ m}\cdot\text{s}^{-1}$, (c) comparison of oil rejection between SS-HFCM and LFS-HFCM at a cross-flow velocity of $1.67 \text{ m}\cdot\text{s}^{-1}$, and the inserted photos of feed and permeates after filtration by LFS-HFCM at a cross-flow velocity of $1.67 \text{ m}\cdot\text{s}^{-1}$: (1) first time filtration, (2) second time filtration after membrane regeneration and (3) tap water and (d) comparison of permeability and oil rejection between the existing state-of-the-art ceramic membranes reported in the literature and high flux spinel based ceramic membranes fabricated in this work.

Besides possessing excellent rejection, the LFS-HFCMs prepared in this work have a much higher flux than inorganic ceramic membranes described in the literature (Fig. 4d and Table 1).

Although they have very high oil rejection all above 91%, the flux of the LFS-HFCMs in our work is ~5, ~3.6, ~6, ~7.8 and ~85 times higher than those of TiO₂-mullite, SiC, α-Si₃N₄, GO-Al₂O₃ and ZrO₂, respectively. The LFS-HFCMs in our work have a highly asymmetrical structure consisting of very thin sponge-like layer (16%) and long finger-like macro-voids (84%) with a total membrane thickness of only 0.38 mm (Fig. 2b2). Such a rationally designed membrane structure could significantly reduce permeation resistance with much shorter liquid transport path, endowing much higher permeation flux while still maintaining high rejection.

3.3.2. Membrane fouling mechanism

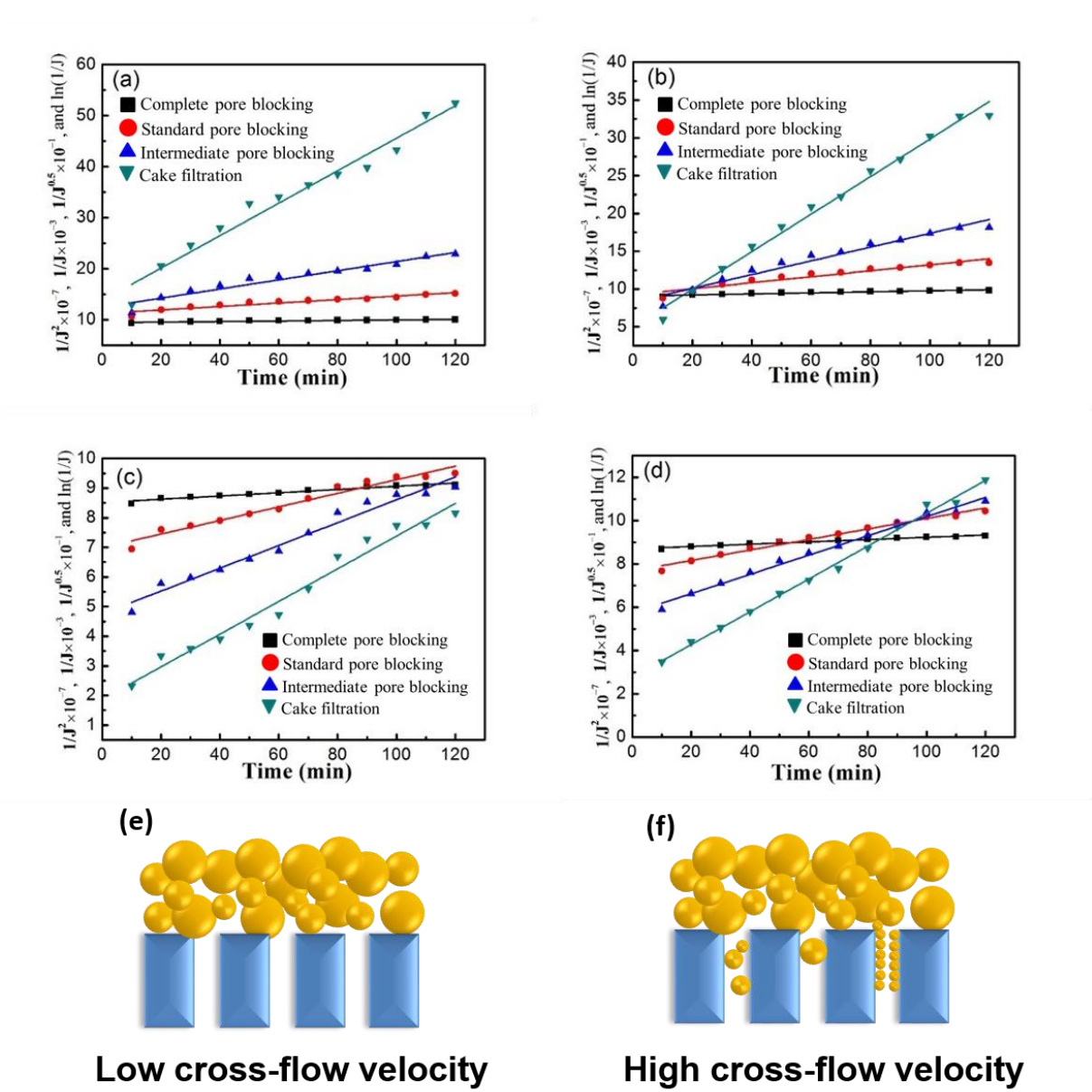


Fig. 5. Plots of flux functions vs time for four different pore blocking models at a fixed trans-membrane pressure of 0.1 bar: (a) LFS-HFCM at a cross-flow velocity of $0.56 \text{ m}\cdot\text{s}^{-1}$, (b) LFS-HFCM at a cross-flow velocity of $1.12 \text{ m}\cdot\text{s}^{-1}$, (c) LFS-HFCM at a cross-flow velocity of $1.67 \text{ m}\cdot\text{s}^{-1}$, and (d) SS-HFCM at a cross-flow velocity of $1.67 \text{ m}\cdot\text{s}^{-1}$, and fouling mechanism at low cross-flow and high cross-flow velocities for O/W emulsion separation: (e) cake formation and (f) cake formation and pore blocking.

Fig. 5 presents the correlations of different pore blocking models for SS-HFCM and LFS-HFCM at various cross-flow velocities ($0.56, 1.12, 1.67 \text{ m}\cdot\text{s}^{-1}$) with a constant applied pressure of 0.1 bar. The cake filtration model offers the best fit as compared with other models for LFS-HFCM at two low cross-flow velocities ($0.56, 1.12 \text{ m}\cdot\text{s}^{-1}$). This is also supported by the parameters of four filtration models, such as correlation coefficients (R^2), slope and initial flux values summarized in **Table S6**. Correlation coefficients (R^2) values for the cake filtration model is the highest value among those for other models, indicating that this model appears to be the best fit in this work for predicting the fouling mechanism of O/W emulsion separation. Similar results have been reported by Kumar et al. (Kumar et al., 2015), who also point out that the best fouling model for oily wastewater microfiltration by tubular ceramic membrane is the cake filtration model. When cross-flow velocity increases up to $1.67 \text{ m}\cdot\text{s}^{-1}$, R^2 values of four models are much closer, especially for SS-HFCM, indicating that pore blocking is partially responsible for flux decline at higher cross-flow velocities. It is believed that at higher cross-flow velocities, the membrane fouling can be explained better with a combined model (pore blocking and cake filtration mechanism) (Corbatón-Báguena et al., 2015; Rezaei et al., 2011; Yazdanshenas et al., 2010). To explain this phenomenon in a better way, we also have calculated Reynolds number (Re) at different cross-flow velocities (**Table S7**). As can be seen from **Table S7**, Re value increases with cross-flow velocities. The larger the Re, the higher the shear stress. Accordingly, increasing cross-flow velocity resulted in an increase of mass transfer coefficient, decreasing mass boundary layer. At cross-flow velocities of 0.56 and $1.12 \text{ m}\cdot\text{s}^{-1}$, the laminar flow model dominated in the hollow fiber. Thus the mass boundary layer was still very thick and a cake

layer was easily formed on the membrane surface. At a higher cross-flow velocity ($1.67 \text{ m}\cdot\text{s}^{-1}$), the flow model was in a transition state between laminar and turbulent, where the thickness of boundary layer decreased significantly but still existed on the membrane surface. Rezaei et al. (Rezaei et al., 2011) also found that there was a more significant reduction of cake resistance with Reynolds numbers higher than 1750. On the other hand, the permeate flux increased at higher cross-flow velocity as the boundary layer became thinner, which resulted in a higher permeate drag force imparted on oil droplets and consequently caused the deformation and squeezing of oil droplets across the membrane pores (Tummons et al., 2017). Kirschner et al. found that when the permeate flux approached and passed a threshold flux, a model combining pore blocking and cake filtration appeared to give the best agreement with experimental data (Kirschner et al., 2019). This phenomenon was also confirmed in a study with SEM images where the blockage of top layer and formation of cake layer above it were both observed (Yazdanshenas et al., 2010). This can also explain the more rapid decline rate of flux and decrease in oil rejection, as observed at the early stages of filtration at a cross flow rate of $1.67 \text{ m}\cdot\text{s}^{-1}$ for SS-HFCM and LFS-HFCM in Fig. 4.

3.3.3. Cost and environment risk assessment

By using bauxite, besides lower stabilization cost than alumina and kaolinite (Fig. S6), our work also demonstrated that a lower cost for membrane fabrication can be achieved compared with other membrane materials such as alumina and zirconia (Fig. S14). This indicates that the use of bauxite and heavy-metal-laden wastes is a promising strategy not only for a more economic and safe heavy-metal stabilization, but lower fabrication cost for membranes, which have outstanding flux and rejection performance for water treatment.

Although spinel has previously been used as a porous membrane for microfiltration and ultrafiltration (Fung and Wang, 2014; Pflanz et al., 1992), considering the presence of metal ions such as Al, Ni, Ca and Fe in the starting materials for membrane preparation, in order to

fully assess any possible environmental risk of the prepared spinel-based HFCMs in wastewater treatment, the concentration of some key metal ions in the permeate was measured (Table S8). Only very low levels of these metal ions were detected, consistently meeting the drinking water criteria issued by World Health Organization (Guidelines for drinking-water quality fourth edition, WHO, 2011). The very low levels of these metal ions present in the permeate are attributable to the stabilization of major component metal ions such as Ni and Al into the spinel crystalline lattice during the ceramic membrane sintering process, along with stabilization of trace amounts of other metal ions such as Ca, Fe and Mg via solid dissolution. Therefore, the spinel-based HFCMs prepared by the waste-to-resource method for recycling of heavy metal-laden solid-state wastes are considered as promising membranes for water treatment from the viewpoints of environment, economic, safety and performance.

4. Conclusions

In this work, a new waste-to-resource conceptual design strategy for the development of cost-effective and high performance robust functional ceramic membranes is presented for not only recycling of wastewater sludge but for the treatment of oil-in-water emulsion wastewater. Besides highly efficient and safe stabilization of heavy metal into ceramic lattice via high temperature sintering, functional ceramic membranes were further structurally designed as stabilized products with excellent oil-in-water separation performance. Two representative membranes: SS-HFCM (fiber 3) and LFS-HFCM (fiber 7) with typically different cross-sectional structures were compared for O/W emulsion separation. LFS-HFCM had a much higher flux than SS-HFCM due to the highly asymmetric structure with a super-high finger-like/sponge-like ratio of ~ 5.25 . The pore blocking model was used to analyze the membrane fouling mechanism. The results indicate that dynamic oil layer formation was the main reason for fouling at low cross-flow velocities, while a combined model of oil layer formation and pore blocking dominated fouling at high cross-flow velocities. Furthermore, compared with existing

state-of-the-art ceramic membranes, the prepared membranes with microfiltration function had better performance but a lower cost, which not only can be directly extended to other separation applications such as the effective removal of bacteria, virus and suspended fine solids from various wastewater streams after further optimization of membrane structure and performance, but also can be considered as robust supports for further fabricating both catalytic membrane reactors and finer-pore separation membranes such as ultrafiltration and nanofiltration membranes for water purification, desalination and even gas separation etc.. Therefore, this method puts forward a new direction for safe and high-value added recycling of heavy metal-laden sludges and shows a promising strategy for treating liquid waste by solid-state waste, achieving dual environmental and economic benefits.

Acknowledgements

This work was financially supported by the National Natural Science Foundation of China (No. 21876020), Youth Top-Notch Talent Program of Talent Project of Revitalizing Liaoning (No. XLYC1807250), Key Project of Liaoning Natural Science Foundation (No. 20180510005), the Fundamental Research Funds for the Central Universities (No. DUT18LAB02 and DUT16RC(3)050), the Haitian Scholar Program from Dalian University of Technology, and the 111 Program of Introducing Talents of Discipline to Universities (No. B13012). We would like to thank Prof. Stephen R. Gray from Victoria University, Australia for his valuable suggestions and help on manuscript corrections and comments.

Appendix A. Supplementary data

Supplementary data related to this article can be found in the Supporting Information

References

- Abadi, S.R.H., Sebzari, M.R., Hemati, M., Rekabdar, F., Mohammadi, T., 2011. Ceramic membrane performance in microfiltration of oily wastewater. *Desalination* 265 (1-3), 222-228.
- Abadikhah, H., Zou, C.-N., Hao, Y.-Z., Wang, J.-W., Lin, L., Khan, S.A., Xu, X., Chen, C.-S., Agathopoulos, S., 2018. Application of asymmetric Si₃N₄ hollow fiber membrane for cross-flow microfiltration of oily waste water. *J. Eur. Ceram. Soc.* 38 (13), 4384-4394.
- Ahmad, A., Ismail, S., Bhatia, S., 2005. Ultrafiltration behavior in the treatment of agro-industry effluent: pilot scale studies. *Chem. Eng. Sci.* 60 (19), 5385-5394.
- Alias, N.H., Jaafssar, J., Samitsu, S., Matsuura, T., Ismail, A., Othman, M., Rahman, M.A., Othman, N., Abdullah, N., Paiman, S., 2018. Photocatalytic nanofiber-coated alumina hollow fiber membranes for highly efficient oilfield produced water treatment. *Chem. Eng. J.* 360, 1437-1446
- Chang, Q., Zhou, J.-e., Wang, Y., Liang, J., Zhang, X., Cerneaux, S., Wang, X., Zhu, Z., Dong, Y., 2014. Application of ceramic microfiltration membrane modified by nano-TiO₂ coating in separation of a stable oil-in-water emulsion. *J. Membr. Sci.* 456, 128-133.
- Chen, M.L., Zhu, L., Dong, Y.C., Li, L.L., Liu, J., 2016. Waste-to-resource strategy to fabricate highly porous whisker-structured mullite ceramic membrane for simulated oil-in-water emulsion wastewater treatment. *ACS Sustain. Chem. Eng.* 4 (4), 2098-2106.
- Christensen, T.H., Kjeldsen, P., Bjerg, P.L., Jensen, D.L., Christensen, J.B., Baun, A., Albrechtsen, H.-J., Heron, G., 2001. Biogeochemistry of landfill leachate plumes. *Appl. Geochem.* 16 (7-8), 659-718.
- Chung, F.H., 1974. Quantitative interpretation of X-ray diffraction patterns of mixtures. II. Adiabatic principle of X-ray diffraction analysis of mixtures. *J. Alloy. Compd.* 7 (6), 526-531.
- Corbatón-Báguena, M.-J., Álvarez-Blanco, S., Vincent-Vela, M.-C., 2015. Fouling mechanisms of ultrafiltration membranes fouled with whey model solutions. *Desalination* 360, 87-96.
- Dong, Y., Lin, B., Xie, K., Wang, S., Ding, H., Fang, D., Liu, X., Meng, G., 2009. Cost-effective macroporous mullite-corundum ceramic membrane supports derived from the industrial grade powder. *J. Alloys Compd.* 477(1-2), 350-356.
- Dong, Y., Ma, L., Tang, C.Y., Yang, F., Quan, X., Jassby, D., Zaworotko, M.J., Guiver, M.D., 2018. Stable superhydrophobic ceramic-based carbon nanotube composite desalination membranes. *Nano Lett.* 18 (9), 5514-5521.
- Duruibe, J.O., Ogwuegbu, M., Ekwurugwu, J., 2007. Heavy metal pollution and human biotoxic effects. *Int. J. Phys. Sci.* 2 (5), 112-118.
- Fraga, M., Sanches, S., Pereira, V., Crespo, J., Yuan, L., Marcher, J., de Yuso, M.V.M., Rodríguez-Castellón, E., Benavente, J., 2017. Morphological, chemical surface and filtration characterization of a new silicon carbide membrane. *J. Eur. Ceram. Soc.* 37 (3), 899-905.
- Fung, Y.-L.E., Wang, H., 2014. Nickel aluminate spinel reinforced ceramic hollow fibre membrane. *J. Membr. Sci.* 450, 418-424.

- Guo, J., Lou, H., Zhao, H., Chai, D., Zheng, X., 2004. Dry reforming of methane over nickel catalysts supported on magnesium aluminate spinels. *Appl. Catal. A-Gen.* 273 (1-2), 75-82.
- Hu, X., Yu, Y., Zhou, J., Wang, Y., Liang, J., Zhang, X., Chang, Q., Song, L., 2015. The improved oil/water separation performance of graphene oxide modified Al₂O₃ microfiltration membrane. *J. Membr. Sci.* 476, 200-204.
- Hua, F.L., Tsang, Y.F., Wang, Y.J., Chan, S.Y., Chua, H., Sin, S.N., 2007. Performance study of ceramic microfiltration membrane for oily wastewater treatment. *Chem. Eng. J.* 128 (2), 169-175.
- Kingsbury, B.F., Li, K., 2009. A morphological study of ceramic hollow fibre membranes. *J. Membr. Sci.* 328 (1-2), 134-140.
- Kirschner, A.Y., Cheng, Y.-H., Paul, D.R., Field, R.W., Freeman, B.D., 2019. Fouling mechanisms in constant flux crossflow ultrafiltration. *J. Membr. Sci.* 574, 65-75.
- Kumar, R.V., Ghoshal, A.K., Pugazhenti, G., 2015. Elaboration of novel tubular ceramic membrane from inexpensive raw materials by extrusion method and its performance in microfiltration of synthetic oily wastewater treatment. *J. Membr. Sci.* 490, 92-102.
- Leblud, C., Anseau, M., Rupo, E., Cambier, F., Fierens, P., 1981. Reaction sintering of ZnO-Al₂O₃ mixtures. *J. Mater. Sci.* 16 (2), 539-544.
- Lee, S.-J., Kim, J.-H., 2014. Differential natural organic matter fouling of ceramic versus polymeric ultrafiltration membranes. *Water Res.* 48, 43-51.
- Li, L., Dong, X., Dong, Y., Zheng, Y.-M., Zhu, L., Liu, J., 2015a. Thermal conversion of hazardous metal copper via the preparation of CuAl₂O₄ spinel-based ceramic membrane for potential stabilization of simulated copper-rich waste. *ACS Sustain. Chem. Eng.* 3 (11), 2611-2618.
- Li, L., Dong, X., Dong, Y., Zhu, L., You, S.-J., Wang, Y.-F., 2015b. Incorporation of zinc for fabrication of low-cost spinel-based composite ceramic membrane support to achieve its stabilization. *J. Hazard. Mater.* 287, 188-196.
- Li, Q., Elimelech, M., 2004. Organic fouling and chemical cleaning of nanofiltration membranes: measurements and mechanisms. *Environ. Sci. Technol.* 38 (17), 4683-4693.
- Lu, D., Zhang, T., Gutierrez, L., Ma, J., Croué, J.-P., 2016. Influence of surface properties of filtration-layer metal oxide on ceramic membrane fouling during ultrafiltration of oil/water emulsion. *Environ. Sci. Technol.* 50 (9), 4668-4674.
- Obaid, M., Mohamed, H.O., Yasin, A.S., Yassin, M.A., Fadali, O.A., Kim, H., Barakat, N.A.M., 2017. Under-oil superhydrophilic wetted PVDF electrospun modified membrane for continuous gravitational oil/water separation with outstanding flux. *Water Res.* 123, 524-535.
- Pflanz, K.B., Riedel, R., Chmiel, H., 1992. Preparation of spinel ultrafiltration membranes. *Adv. Mater.* 4 (10), 662-665.
- Prince, J.A., Bhuvana, S., Anbharasi, V., Ayyanar, N., Boodhoo, K.V.K., Singh, G., 2016. Ultra-wetting graphene-based PES ultrafiltration membrane – A novel approach for successful oil-water separation. *Water Res.* 103, 311-318.

- Rezaei, H., Ashtiani, F.Z., Fouladitajar, A., 2011. Effects of operating parameters on fouling mechanism and membrane flux in cross-flow microfiltration of whey. *Desalination* 274 (1), 262-271.
- Salahi, A., Gheshlaghi, A., Mohammadi, T., Madaeni, S.S., 2010. Experimental performance evaluation of polymeric membranes for treatment of an industrial oily wastewater. *Desalination* 262 (1-3), 235-242.
- Shih, K., White, T., Leckie, J.O., 2006a. Nickel stabilization efficiency of aluminate and ferrite spinels and their leaching behavior. *Environ. Sci. Technol.* 40 (17), 5520-5526.
- Shih, K., White, T., Leckie, J.O., 2006b. Spinel formation for stabilizing simulated nickel-laden sludge with aluminum-rich ceramic precursors. *Environ. Sci. Technol.* 40 (16), 5077-5083.
- Slack, R., Gronow, J., Voulvoulis, N., 2005. Household hazardous waste in municipal landfills: contaminants in leachate. *Sci. Total Environ.* 337 (1-3), 119-137.
- Song, F., Gu, L., Zhu, N., Yuan, H., 2013. Leaching behavior of heavy metals from sewage sludge solidified by cement-based binders. *Chemosphere* 92 (4), 344-350.
- Tang, Y., Chui, S.S.-Y., Shih, K., Zhang, L., 2011a. Copper stabilization via spinel formation during the sintering of simulated copper-laden sludge with aluminum-rich ceramic precursors. *Environ. Sci. Technol.* 45 (8), 3598-3604.
- Tang, Y., Shih, K., Wang, Y., Chong, T.-C., 2011b. Zinc stabilization efficiency of aluminate spinel structure and its leaching behavior. *Environ. Sci. Technol.* 45 (24), 10544-10550.
- Tummons, E.N., Chew, J.W., Fane, A.G., Tarabara, V.V., 2017. Ultrafiltration of saline oil-in-water emulsions stabilized by an anionic surfactant: Effect of surfactant concentration and divalent counterions. *J. Membr. Sci.* 537, 384-395.
- Vasanth, D., Pugazhenthii, G., Uppaluri, R., 2011. Fabrication and properties of low cost ceramic microfiltration membranes for separation of oil and bacteria from its solution. *J. Membr. Sci.* 379 (1-2), 154-163.
- Vasanth, D., Pugazhenthii, G., Uppaluri, R., 2013. Cross-flow microfiltration of oil-in-water emulsions using low cost ceramic membranes. *Desalination* 320, 86-95.
- Wei, C.C., Chen, O.Y., Liu, Y., Li, K., 2008. Ceramic asymmetric hollow fibre membranes—one step fabrication process. *J. Membr. Sci.* 320 (1-2), 191-197.
- Yang, C., Zhang, G., Xu, N., Shi, J., 1998. Preparation and application in oil–water separation of ZrO₂/α-Al₂O₃ MF membrane. *J. Membr. Sci.* 142 (2), 235-243.
- Yazdanshenas, M., Soltanieh, M., Tabatabaei Nejad, S.A.R., Fillaudeau, L., 2010. Cross-flow microfiltration of rough non-alcoholic beer and diluted malt extract with tubular ceramic membranes: Investigation of fouling mechanisms. *J. Membr. Sci.* 362 (1), 306-316.
- Zhang, L., Wang, X., Shang, X., Tan, M., Ding, W., Lu, X., 2017. Carbon dioxide reforming of methane over mesoporous nickel aluminate/γ-alumina composites. *J. Energy Chem.* 26 (1), 93-100.
- Zhang, X., Lin, B., Ling, Y., Dong, Y., Fang, D., Meng, G., Liu, X., 2010. Highly permeable porous YSZ hollow fiber membrane prepared using ethanol as external coagulant. *J. Alloy. Compd.* 494 (1-2),

366-371.

Zhu, L., Chen, M., Dong, Y., Tang, C.Y., Huang, A., Li, L., 2016. A low-cost mullite-titania composite ceramic hollow fiber microfiltration membrane for highly efficient separation of oil-in-water emulsion. *Water Res.* 90, 277-285.

Zhu, L., Dong, X., Xu, M., Yang, F., Guiver, M.D., Dong, Y., 2019. Fabrication of mullite ceramic-supported carbon nanotube composite membranes with enhanced performance in direct separation of high-temperature emulsified oil droplets. *J. Membr. Sci.* 582, 140-150.